ChemComm

COMMUNICATION

View Article Online
View Journal | View Issue

Cite this: *Chem. Commun.*, 2025, **61**, 3508

Received 29th November 2024,
Accepted 27th January 2025

DOI: 10.1039/d4cc06335j

rsc.li/chemcomm

Solution triggered facile ion-exchange and phase transformation of ternary cesium-copper halide pseudo-perovskites†

Cintia Hajdu,[a] Tamás Sándor Zsigmond,[a] Bence Kutus,[c] Ditta Ungor,[ab] Edit Csapó,[ab] Csaba Janáky *[a] and Gergely Ferenc Samu *[c]

Ternary cesium-copper halide pseudo-perovskites are an emerging class of semiconductors in the field of optoelectronics. Similarly to metal-halide perovskites, by controlling the halide-composition, their emission properties can be fine-tuned. Here, a post-synthetic halide exchange method was employed to alter the halide-composition and thus the emission properties of polycrystalline $Cs_3Cu_2Br_5$ layers.

The crystal structure of $Cs_3Cu_2X_5$ and $CsCu_2X_3$ (X = Br, I, Cl) pseudo-perovskites consists of anionic metal-halides with intercalated monovalent cations.[1] They have gained significant attention as light-emitting diodes,[2–4] photodetectors,[5,6] charged-particle or X-ray scintillators,[7,8] and even as anti-counterfeiting materials.[9] These compounds have the advantages of good thermal and chemical stability,[10] and low toxicity,[11] coupled with simple and cost-effective preparation methods.[12] Their soft lattice can easily undergo lattice distortions after excitation,[13] which results in the formation of self-trapped exciton (STE) states. Light emission through STE states is shifted to notably longer wavelengths compared to the absorption onset (large Stokes shift), eliminating reabsorption completely.[14,15] Furthermore, the large detrapping barrier bestows high quantum efficiencies to STE emission processes.[15]

Composition engineering targeting the halide content can be used to fine-tune the light emission properties (*e.g.*, Stokes shift, photoluminescence quantum yield and lifetime) of pseudo-perovskites.[16–24] This is the result of the large contribution of the *n*p orbital of the halide anions to the band structure.[12,18]

The halide composition of metal halide perovskites can be fine-tuned either during synthesis[25] or by post-synthetic halide exchange methods.[24,26,27] The former method additionally influences the crystallization kinetics[28] of the films (even without halide incorporation)[29] or passivates surface trap states[30] impacting device properties. The latter approach can either preserve the original crystal structure of the starting material[21] or result in a different crystal structure, which can give further control over the optoelectronic properties.[23] The exchange can be performed in the gas,[31] liquid[22–24,32] or solid phase,[33] but in the latter case achieving complete exchange is difficult and often poorly controllable.[13] In the case of films, the use of harsh reaction conditions (*e.g.*, elevated temperatures >70 °C), and long reaction times (few days) are often necessary to achieve complete exchange. In one example, bromide-to-iodide halide exchange was studied in a 75 nm thick $CsPbBr_3$ film, at 75 °C for 40 minutes. If the layer thickness was increased to 350 nm, the solution temperature had to be increased to 120 °C, and the immersion time extended to 480 min.[34] Mechanistic studies revealed that the exchange is kinetically driven by ion diffusion within the layers and the surrounding environment.[13,35,36] From the layer side, the presence of crystal defects plays a key role in the halide exchange process, as they govern ion migration pathways within the material, and reduce the activation energy of diffusion. Similarly, temperature also plays a role according to the Arrhenius equation.[13,37] Applying electrical bias can facilitate ion migration[38,39] and the created vacancies can further accelerate this process. From the environment (solution) side, the difference in halide solubility has a detrimental effect on the rate of halide exchange.[13,40]

So far, halide exchange in pseudo-perovskites is an unexplored area. To the best of our knowledge, only Cl^- to I^- post-synthetic halide exchange has been demonstrated on $Cs_3Cu_2Cl_5$ single crystals.[41] The process was performed with hydrogen-iodide injection at 60 °C in a phosphorous acid containing ethanol solution. Additionally, a 0D–1D phase transition ($Cs_3Cu_2I_5$–$CsCu_2I_3$) was shown for these materials by immersing them in solvents with different polarity.[9,42,43]

[a] *Department of Physical Chemistry and Materials Science, Interdisciplinary Excellence Centre, University of Szeged, Aradi Square 1, Szeged, H-6720, Hungary. E-mail: janaky@chem.u-szeged.hu*
[b] *MTA-SZTE Lendület "Momentum" Noble Metal Nanostructures Research Group, University of Szeged, Rerrich Béla Square 1, Szeged, H-6720, Hungary*
[c] *Department of Molecular and Analytical Chemistry, University of Szeged, Dóm Square 7-8, Szeged, H-6721, Hungary. E-mail: samugf@chem.u-szeged.hu*

† Electronic supplementary information (ESI) available. See DOI: https://doi.org/10.1039/d4cc06335j

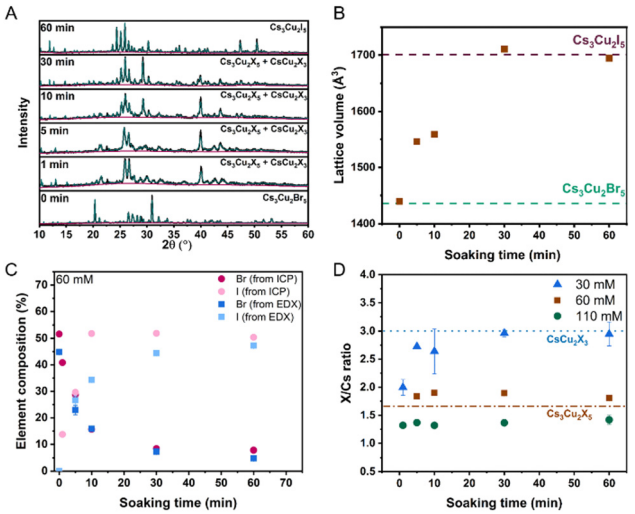

Fig. 1 (A) XRD characterization of the $Cs_3Cu_2Br_5$ layers before and after halide exchange. The blue lines represent Le Bail fitting of the data. (B) The effect of soaking time on the calculated lattice volume from Le Bail fitting for the $Cs_3Cu_2X_5$ portion of the layers. (C) The effect of soaking time on the bromide and iodide content of the films derived from ICP-MS and EDX analysis of the films. (D) Soaking time dependence of the halide (X) to cesium atomic ratio of the layers determined from EDX measurement. The blue dotted line represents the case of $CsCu_2X_3$ composition, while the brown dashed line the $Cs_3Cu_2X_5$ composition. The error bars represent three different spots on one layer. During all experiments (A) and (C) 60 mM CsI in MeOH soaking solution was used.

In this work, we studied the bromide-to-iodide halide exchange process in a $Cs_3Cu_2Br_5$ polycrystalline film, with 10 μm thickness (details of the preparation can be found in the ESI†). We performed the halide exchange in the liquid phase, by immersing the $Cs_3Cu_2Br_5$ layers in CsI-containing methanol solutions at room temperature (Fig. S1, ESI†). The effect of the CsI concentration and soaking time on the crystal structure, elemental composition, and luminescence properties was studied. XRD (X-ray diffraction) patterns were recorded to monitor the effect of halide exchange on the crystal structure of the $Cs_3Cu_2Br_5$ layers (Fig. 1A and Fig. S2, ESI†). After soaking the layers in 60 mM CsI solution (Fig. 1A), a complex transformation occurred. The emergence of new reflections, and shifts of existing reflections to lower 2 theta values were both observed. Le Bail fitting[44] of the XRD patterns revealed that after 5–30 min of soaking, two crystal forms were coexisting. Apart from mixed $Cs_3Cu_2Br_{5-x}I_x$ (*Pnma*) phases, the emergence of $CsCu_2X_3$ (*Cmcm*) could be observed. After 60 min of immersion the transformation of the film was complete, and only reflections from the $Cs_3Cu_2I_5$ phase could be detected. The individual lattice parameters (Fig. S3A, ESI†) and unit cell volume (Fig. 1B) of the halide-exchanged $Cs_3Cu_2Br_{5-x}I_x$ layers were extracted from the fits of the patterns. The gradual increase in the lattice volume over time suggests the exchange of the smaller bromide (r = 196 pm) with larger iodide (r = 220 pm) in the lattice. The determined lattice volume (Fig. 1B) stabilized after 30 min, which signals the completion of the halide exchange process (at least in the probing depth of the XRD measurements). These results were also corroborated by the composition analysis of the exchanged layers both with ICP-MS (inductively coupled plasma mass spectrometry) (Fig. 1C and Fig. S4, Tables S1–S3, ESI†) and EDX (energy dispersive X-ray spectroscopy) (Fig. 1C and Table S4, ESI†) measurements. After 30 min almost all bromide was exchanged to iodide in the layers. Interestingly, in the case of 30 mM CsI solutions, the XRD patterns (Fig. S2A, ESI†) revealed a slower transformation of the soaked layers, which stopped at the formation of iodide-rich $Cs_3Cu_2X_3$ films. In stark contrast, when using 110 mM (saturated) CsI solutions, the crystal structure of the starting $Cs_3Cu_2Br_5$ was retained (Fig. S2B, ESI†) and no lattice volume change was observed (Fig. S5A, ESI†), while the formation of $Cs_3Cu_2I_5$ phase was prevalent throughout the experiment as corroborated by ICP-MS and EDX measurements (Tables S3 and S6, ESI†). In the case of the 30 mM CsI solution, the iodide incorporation, at the expense of bromide, was confirmed (Tables S1 and S5, ESI†). Interestingly, a lower iodide content was achieved with the 110 mM CsI soaking solution (Tables S3 and S6, ESI†). This, together with the XRD results, points toward the formation of a layered structure, where iodide incorporation is confined to the outmost regions of the films. Detailed discussion of the ICP-MS results can be found in the ESI.†

To quantify the change in the surface halide composition of the layers, we calculated the overall halide/cesium ratio of the films (Fig. 1D) from EDX. When concentrated solutions (60 mM and 110 mM) were used, the halide/Cs ratio retained its value (which was close to the expected 1.67 value in $Cs_3Cu_2X_5$ compounds). In the case of the dilute 30 mM CsI solution, the halide/Cs ratio shifted to higher values (close to the expected 3.0 value in the $CsCu_2X_3$ compounds). These results are in line with XRD measurements, supporting the change of crystal structure in the 30 mM CsI case.

The schematic representation of the proposed mechanism of the halide exchange process is summarized in Fig. 2. In dilute CsI solution the halide exchange is coupled with a 0D–1D phase transition between $Cs_3Cu_2Br_5$ and $Cs_3Cu_2I_3$. The reason for this compositional/structural change can be the CsBr leaching from the layers to the solution phase (as revealed by ICP-MS). This is supported by the negligible weight loss of the films after immersion in the 30 mM CsI solution (Table S7, ESI†). As the iodide/bromide exchange should increase the weight of the films,

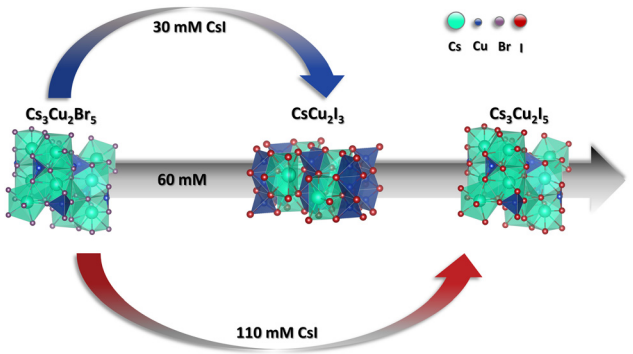

Fig. 2 Summary of the different structures controlled by the halide exchange method.

a slight dissolution seems necessary to induce the 0D–1D transformation process. When a more concentrated CsI soaking solution is employed, the transition can progress gradually through a mixed phase of $CsCu_2I_3$ and $Cs_3Cu_2I_5$ to phase pure $Cs_3Cu_2I_5$. In contrast, when saturated CsI solution is used, no phase change occurs, however examining the unit cell dimensions, $Cs_3Cu_2Br_5$ and surface $Cs_3Cu_2I_5$ can be identified.

To observe the morphological changes accompanying the halide exchange process, top-down SEM (scanning electron microscopy) images were recorded. Before the soaking procedure, granular $Cs_3Cu_2Br_5$ layers were observed (Fig. S6A, ESI†). Upon immersion in 60 mM exchange solution for 10 minutes of soaking time, a mixture of grains and rods can be observed (Fig. S6B, ESI†). The rod-like morphology is characteristic of the 1D $CsCu_2X_3$ phase,[12] signalling that a mixed $Cs_3Cu_2Br_{5-x}I_x$/$CsCu_2I_3$ composition was obtained. After prolonged soaking time, the rods disappeared from the surface and only grains can be observed (Fig. S7, ESI†). In the case of the less concentrated CsI solution (30 mM), only rods were present (Fig. S6C, ESI†), throughout the entirety of the process (Fig. S7, ESI†). Interestingly, by examining the stack of rods, the original grains of the parent layers can still be recognized. In a similar fashion, when the saturated 110 mM CsI solution was used, only the surface of the layers was exchanged, preserving the granular structure of the parent $Cs_3Cu_2X_5$ material (Fig. S6D and S7, ESI†).

To probe the effect of the halide exchange process on the light emission properties of the layers, steady state PL (photoluminescence) spectra were recorded (Fig. 3). The initial $Cs_3Cu_2Br_5$ layers had a PL peak maximum position of 460 nm and a PLQY of $\sim 14 \pm 3\%$. After the layers were immersed in the 30 mM CsI solution, a rapid decrease of the PL intensity could be observed (Fig. 3A) at the characteristic wavelength of the parent $Cs_3Cu_2Br_5$. This was accompanied with an increase in PL intensity at 570 nm, which corresponds to the formation of $CsCu_2I_3$. The difference in the PL intensity is the result of the low PLQY of the forming $CsCu_2I_3$ ($\sim 2.2\%$). In stark contrast, when performing the halide exchange with concentrated exchange solutions (60 mM and 110 mM) a rapid increase in the PL intensity (Fig. 3B and C) could be observed, together with a shift of the PL maximum to lower wavelengths (~ 440 nm), characteristic of the formation of $Cs_3Cu_2I_5$ (high PLQY $\sim 72\%$).

To quantify the change in the light emission properties, we integrated the PL peaks (Fig. S8, ESI†) and determined the absolute PLQY (Fig. 4A and Fig. S9, ESI†) of the layers. Both measurements revealed that the highest PLQY (73%) belongs to the samples treated with the 60 mM soaking solution, where $Cs_3Cu_2I_5$ was obtained (deduced from materials characterization). This value is comparable to a pure $Cs_3Cu_2I_5$ reference layer (78%), prepared by the spray-coating method. In a similar manner, the halide exchange carried out in the saturated 110 mM CsI solution improves the PLQY to 38%. Interestingly, the initial period of soaking (1 minute) in the concentrated solutions (60 mM and 110 mM) preserves the peak position of $Cs_3Cu_2Br_5$ (Fig. 4B), while drastically increasing the PLQY to $\sim 35\%$. One possible reason can be the trap state passivation of the $Cs_3Cu_2Br_5$ layer by the surface exchange to $Cs_3Cu_2I_5$. Ultimately, however, the PL maximum shifts to 440 nm in these cases as seen in Fig. 4B. The halide exchange process influences the decay of the PL response as well (Fig. 4C). We fitted the decay traces by a multiexponential function (Table S8, ESI†) and calculated the average PL lifetime (Fig. 4D, Table S9, ESI†), which is independent of the model used. This approach is justified by the multiphasic nature of the samples, which makes identifying separate processes unreliable. The initial $Cs_3Cu_2Br_5$ layers have the longest average lifetime (10.7 ± 0.2 μs). After performing the halide exchange in the 60 mM CsI solution, the decay of the PL signal gradually accelerates. The shortest lifetime of 1.13 ± 0.02 μs was determined for the sample after 60 min soaking. This value is in good correlation with literature data for phase pure $Cs_3Cu_2I_5$ further signalling complete halide exchange.

To summarize our work, we successfully prepared $Cs_3Cu_2Br_5$ pseudo-perovskite layers and demonstrated bromide/iodide exchange with a simple room temperature solution phase approach. Depending on the concentration of the CsI exchange solution, both simple halide exchange and a 0D–1D transition were achieved. The halide exchange could be either complete or confined to the $Cs_3Cu_2Br_5$ surface. In all cases, the formed $Cs_3Cu_2I_5$ improved the PLQY of the layers compared to the parent $Cs_3Cu_2Br_5$. When full halide exchange was performed, a high PLQY of 73% was achieved, which is comparable to a reference $Cs_3Cu_2I_5$ sample. The halide exchange has a long-lasting effect as the increased PLQY still persists even after 1 year of storage (Table S10, ESI†). As an outlook this simple,

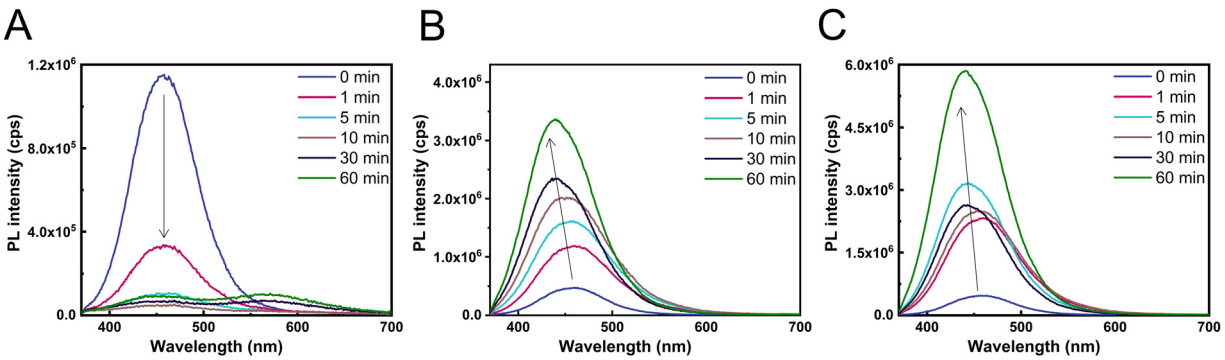

Fig. 3 Steady state PL spectra of the films after performing the halide exchange where, the CsI/MeOH concentration (A) 30 mM, (B) 60 mM and (C) 110 mM was used. The excitation wavelength was 290 nm in all cases.

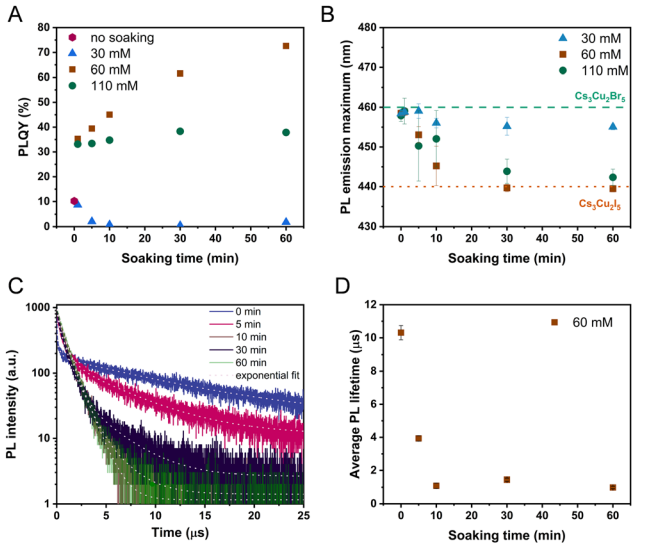

Fig. 4 The effect of halide exchange on the PL properties. Soaking time dependence of (A) PLQY. The red hexagon represents a $Cs_3Cu_2Br_5$ sample before immersion. (B) The PL peak maximum shift of the soaked layers. Error bars represent measurements for at least three layers. (C) PL decay traces of $Cs_3Cu_2Br_5$ films immersed in the 60 mM CsI solution. The traces were recorded with 300 nm excitation at the emission maximum of the layers. (D) Soaking time dependence of the intensity averaged PL lifetime.

fast method could be used to improve and precisely control the optoelectronic properties of $Cs_3Cu_2Br_5$ layers. Notably, the method can form layered structures that could be used in different light/radiation detection applications.

The authors thank Ádám Balog for SEM/EDX measurements. This work was supported by TKP-2021-NVA-19 financed by the National Research, Development and Innovation Fund of the Ministry of Culture and Innovation of Hungary and by the National Research, Development and Innovation Office (NKFIH) through the FK-138888 project and the ERA-NET COFUND/EJP COFUND Program with co-funding from the European Union Horizon 2020 research and innovation program and the NKFIH (2019-2.1.7-ERA-NET-2021-00025).

Data availability

The data supporting this article have been included as part of the ESI.†

Conflicts of interest

There are no conflicts to declare.

Notes and references

1 Y. Nah, D. Solanki and D. H. Kim, *Cell Rep. Phys. Sci.*, 2022, **3**, 101171.
2 T. Jun, K. Sim, S. Iimura, M. Sasase, H. Kamioka, J. Kim and H. Hosono, *Adv. Mater.*, 2018, **30**, 1804547.
3 L. Wang, Z. Shi, Z. Ma, D. Yang, F. Zhang, X. Ji, M. Wang, X. Chen, G. Na, S. Chen, D. Wu, Y. Zhang, X. Li, L. Zhang and C. Shan, *Nano Lett.*, 2020, **20**, 3568–3576.
4 X. Liu, Y. Yu, F. Yuan, C. Zhao, H. Dong, B. Jiao and Z. Wu, *ACS Appl. Mater. Interfaces*, 2020, **12**, 52967–52975.
5 Z. X. Zhang, C. Li, Y. Lu, X. W. Tong, F. X. Liang, X. Y. Zhao, D. Wu, C. Xie and L. B. Luo, *J. Phys. Chem. Lett.*, 2019, **10**, 5343–5350.
6 Y. Li, Z. Shi, L. Wang, Y. Chen, W. Liang, D. Wu, X. Li, Y. Zhang, C. Shana and X. Fang, *Mater. Horiz.*, 2020, **7**, 1613–1622.
7 M. Hunyadi, G. F. Samu, L. Csige, A. Csík, C. Buga and C. Janáky, *Adv. Funct. Mater.*, 2022, **32**, 2206645.
8 L. Lian, M. Zheng, W. Zhang, L. Yin, X. Du, P. Zhang, X. Zhang, J. Gao, D. Zhang, L. Gao, G. Niu, H. Song, R. Chen, X. Lan, J. Tang and J. Zhang, *Adv. Sci.*, 2020, **7**, 2000195.
9 X. Zhang, B. Zhou, X. Chen and W. W. Yu, *Inorg. Chem.*, 2022, **61**, 399–405.
10 F. Zeng, Y. Guo, W. Hu, Y. Tan, X. Zhang, J. Yang, Q. Lin, Y. Peng, X. Tang, Z. Liu and Z. Yao, *J. Lumin.*, 2020, **223**, 117178.
11 T. D. Creason, T. M. McWhorter, Z. Bell, M. H. Du and B. Saparov, *Chem. Mater.*, 2020, **32**, 6197–6205.
12 Z. Guo, J. Li, R. Pan, J. Cheng, R. Chen and T. He, *Nanoscale*, 2020, **12**, 15560–15576.
13 H. Jiang, S. Cui, Y. Chen and H. Zhong, *Nano Sel.*, 2021, **2**, 2040–2060.
14 S. Li, J. Luo, J. Liu and J. Tang, *J. Phys. Chem. Lett.*, 2019, **10**, 1999–2007.
15 B. Zhang, X. Wu, S. Zhou, G. Liang and Q. Hu, *Front. Optoelectron.*, 2021, **14**, 459–472.
16 R. Roccanova, A. Yangui, H. Nhalil, H. Shi, M. H. Du and B. Saparov, *ACS Appl. Electron. Mater.*, 2019, **1**, 269–274.
17 G. F. Samu, T. S. Zsigmond, C. Hajdu, M. Hunyadi, L. Csige, A. Csík, J. Kopniczky, B. Hopp and C. Janáky, *Adv. Opt. Mater.*, 2023, **11**, 2300825.
18 J. S. Manser, J. A. Christians and P. V. Kamat, *Chem. Rev.*, 2016, **116**, 12956–13008.
19 D. Zhang, Y. Yang, Y. Bekenstein, Y. Yu, N. A. Gibson, A. B. Wong, S. W. Eaton, N. Kornienko, Q. Kong and M. Lai, *J. Am. Chem. Soc.*, 2016, **138**, 7236–7239.
20 L. Han, B. Sun, C. Guo, G. Peng, H. Chen, Z. Yang, N. Li, Z. Ci and Z. Jin, *Adv. Opt. Mater.*, 2022, **10**, 1–9.
21 G. Nedelcu, L. Protesescu, S. Yakunin, M. I. Bodnarchuk, M. J. Grotevent and M. V. Kovalenko, *Nano Lett.*, 2015, **15**, 5635–5640.
22 M. Imran, V. Caligiuri, M. Wang, L. Goldoni, M. Prato, R. Krahne, L. D. Trizio and L. Manna, *J. Am. Chem. Soc.*, 2018, **140**, 2656–2664.
23 N. Pellet, J. Teuscher, J. Maier and M. Grätzel, *Chem. Mater.*, 2015, **27**, 2181–2188.
24 Q. A. Akkerman, V. D'Innocenzo, S. Accornero, A. Scarpellini, A. Petrozza, M. Prato and L. Manna, *J. Am. Chem. Soc.*, 2015, **137**, 10276–10281.
25 S. Ye, M. Zhao, J. Song and J. Qu, *Nano Res.*, 2018, **11**, 4654–4663.
26 P. Ramasamy, D. H. Lim, B. Kim, S. H. Lee, M. S. Lee and J. S. Lee, *Chem. Commun.*, 2016, **52**, 2067–2070.
27 X. He, P. Liu, S. Wu, Q. Liao, J. Yao and H. Fu, *J. Mater. Chem. C*, 2017, **5**, 12707–12713.
28 J. Kim, S. Park, Y. Lee, H. Hosono, B. Park and J. Kim, *SusMat*, 2023, **3**, 821–833.
29 J. Qiu, *et al.*, *SusMat*, 2023, **3**, 894–908.
30 Y. Xia, M. Zhu, L. Qin, C. Zhao, D. Hong, Y. Tian, W. Yan and Z. Jin, *Energy Mater.*, 2023, **3**, 300004.
31 D. Solis-Ibarra, I. C. Smith and H. I. Karunadasa, *Chem. Sci.*, 2015, **6**, 4054–4059.
32 V. Thampy and K. H. Stone, *Inorg. Chem.*, 2020, **59**, 13364–13370.
33 Y. Liu, F. Li, Q. Li, K. Yang, T. Guo, X. Li and H. Zeng, *ACS Photonics*, 2018, **5**, 4504–4512.
34 J. B. Hoffman, A. L. Schleper and P. V. Kamat, *J. Am. Chem. Soc.*, 2016, **138**, 8603–8611.
35 C. Eames, J. M. Frost, P. R. F. Barnes, B. C. O'Regan, A. Walsh and M. S. Islam, *Nat. Commun.*, 2015, **6**, 2–9.
36 A. Walsh, D. O. Scanlon, S. Chen, X. G. Gong and S. Wei, *Angew. Chem.*, 2015, **127**, 1811–1814.
37 P. V. Kamat and M. Kuno, *Acc. Chem. Res.*, 2021, **54**, 520–531.
38 G. F. Samu, A. Balog, F. De Angelis, D. Meggiolaro, P. V. Kamat and C. Janaky, *J. Am. Chem. Soc.*, 2019, **141**, 10812–10820.
39 Z. Xu, R. A. Kerner, J. J. Berry and B. P. Rand, *Adv. Funct. Mater.*, 2022, **32**, 2203432.
40 G. D. Moon, S. Ko, Y. Xia and U. Jeong, *ACS Nano*, 2010, **4**, 2307–2319.
41 D. Shen, X. Wang, X. Zhang, Y. Liu, Y. Shi, X. Li, X. Chen and Y. Zhang, *ACS Appl. Opt. Mater.*, 2023, **1**, 435–441.
42 S. Liu, Y. Yue, X. Zhang, C. Wang, G. Yang and D. Zhu, *J. Mater. Chem. C*, 2020, **8**, 8374–8379.
43 W. Cui, J. Zhao, L. Wang, P. Lv, X. Li, Z. Yin, C. Yang and A. Tang, *J. Phys. Chem. Lett.*, 2022, **13**, 4856–4863.
44 B. H. Toby and R. B. Von Dreele, *J. Appl. Crystallogr.*, 2013, **46**, 544–549.